Leptogenesis and eV scale sterile neutrino

Srubabati Goswami,[1,*] Vishnudath K. N.,[2,†] Ananya Mukherjee,[3,‡] and Nimmala Narendra[1,§]

[1]*Physical Research Laboratory, Theoretical Physics Division, Ahmedabad 380009, India*
[2]*The Institute of Mathematical Sciences, C.I.T. Campus, Taramani, Chennai 600 113, India*
[3]*Department of Physics, University of Calcutta, 92 Acharya Prafulla Chandra Road, Kolkata 700 009, India*

(Received 21 December 2021; accepted 6 May 2022; published 26 May 2022)

We consider the minimal extended seesaw model that can accommodate an eV scale sterile neutrino. The scenario also includes three heavy right-handed neutrinos in addition to the light-sterile neutrino. In this model, the active-sterile mixing acts as nonunitary parameters. If the values of these mixing angles are of $\mathcal{O}(0.1)$, the model introduces deviation of the Pontecorvo-Maki-Nakagawa-Sakata matrix from unitarity to this order. We find that the oscillation data from various experiments impose an upper bound on the lightest heavy neutrino mass scale as $\sim 10^{11}$ GeV in the context of this model. We study *vanilla* leptogenesis in this scheme, where the decay of the heavy right-handed neutrinos in the early Universe can give rise to the observed baryon asymmetry. Here, even though the eV scale sterile neutrino does not participate directly in leptogenesis, its effect is manifested through the nonunitary effects. We find that the parameter space that can give rise to successful leptogenesis is constrained by the bounds on the active-sterile mixing as obtained from the global analysis.

DOI: 10.1103/PhysRevD.105.095040

I. INTRODUCTION

Many short-baseline experiments suggest the existence of at least one light-sterile neutrino of mass in the eV scale. The first hint for this came from the $\overline{\nu_\mu} \to \overline{\nu_e}$ searches in the Liquid Scintillation Neutrino Detector (LSND) experiment [1]. Recently, the Mini Booster Neutrino Experiment (MiniBooNE) experiment also confirmed this from the excess of the electronlike events [2]. Earlier, the reactor [3,4] and the gallium [5–8] anomalies also indicated the presence of an extra sterile neutrino that mixes with the three active flavor states of the Standard Model (SM). For a recent analysis, see [9]. The $3+1$ picture, which was first introduced in [10], is the minimal scheme that can explain these anomalies. However, no signal of a fourth sterile neutrino has been reported in the disappearance experiments using neutrinos from reactors and accelerators [11]. The results of the fit of short-baseline neutrino oscillation data in the framework of $3+1$ active-sterile neutrino mixing are given in [12,13]. See [14] for a recent review on the status and phenomenology of an eV scale sterile neutrino.[1] Also, note that the recent results from the analysis of the three years of data from MicroBooNE showed no excess of electrons. However, this does not yet conclusively prove that a sterile neutrino solution to MiniBooNE data is ruled out [20]. Also, the analysis done in Ref. [21] shows that the oscillations to a sterile neutrino is still possible with $\Delta m^2_{14} \sim 1.5$ eV^2 and $\sin^2\theta_{14} \gtrsim 0.1$ for the intrinsic electron neutrinos in the beam.

Theoretical models that explain nonzero active neutrino masses and can simultaneously incorporate an eV scale sterile neutrino have been proposed, for instance, in [22–25]. An elegant scheme to accommodate a light-sterile neutrino within the type-I seesaw framework is the minimal extended seesaw (MES) discussed in [26]. In the MES scheme, the SM is extended by three heavy Majorana right-handed neutrinos (RHNs) ν_R, whose masses are $\sim\mathcal{O}(10^{12})$ GeV, and another gauge singlet fermion ν_s. Among the three RHNs, two are responsible for making two SM neutrinos massive, whereas the third one gives mass to the light-sterile neutrino. In this model, the mixing between the active neutrinos and the light-sterile neutrino act as the nonunitary

*sruba@prl.res.in
†vishnudathkn@imsc.res.in
‡ananyatezpur@gmail.com
§nnarendra@prl.res.in

[1]Note that an eV scale sterile neutrino is disfavored by cosmology in general. The secret interaction model of sterile neutrinos proposed in [15] to ameliorate the situation was also disfavored later [16–18]. However, the recent analysis done in [19] with a pseudoscalar interaction admits a sterile neutrino of mass ~1 eV.

parameters characterizing the deviation from unitarity of the Pontecorvo-Maki-Nakagawa-Sakata (PMNS) matrix. Several works have attempted to implement this scheme in the context of discrete flavor symmetric groups such as A_4 [27–29].

In addition to explaining the nonzero neutrino masses and mixing, the seesaw mechanism can also address the issue of the baryon asymmetry of the Universe to which the SM does not have an answer [30]. The comoving baryon asymmetry of the Universe is given as

$$Y_B = \frac{(n_B - n_{\bar{B}})}{s}, \tag{1.1}$$

where n_B and $n_{\bar{B}}$ are the number densities of baryons and antibaryons, respectively, and s is the entropy density. The combined analysis of the data from measurements of cosmic microwave background and large scale structure indicates a 3σ range for the baryon asymmetry of the Universe as [31]

$$Y_B = (8.52\text{–}8.93) \times 10^{-11}. \tag{1.2}$$

In the type-I seesaw model, the out-of-equilibrium decay of the heavy Majorana RHNs in the early Universe can generate a lepton asymmetry, which in turn can be converted into a baryon asymmetry via the nonperturbative sphaleron process [32].

We study leptogenesis in the context of the MES model in this work. Specifically, we ask the question if the light-sterile neutrino plays any role in leptogenesis. On a first look, it might appear to one as if the light-sterile neutrino plays absolutely no role in leptogenesis. But on a closer analysis, one can find that the large mixing between the eV scale sterile and active neutrinos can have an impact on leptogenesis. In fact, the standard loop diagrams for the leptogenesis is generated by the dimension-five operator and the inclusion of the nonunitarity effects will correspond to the inclusion of the contribution due to the dimension-six operator. This has been studied at the operator level in the context of a three family low scale seesaw in Ref. [33]. One can also study the nonunitarity effects in leptogenesis by using the Casas-Ibarra (CI) parametrization [34] for the neutrino Yukawa coupling y_ν (or, equivalently, the neutrino Dirac mass term M_D). The expression for the CP asymmetry in leptogenesis depends on y_ν, and in CI parametrization, y_ν can be expressed in terms of the $U_{\rm PMNS}$ matrix, the light and heavy neutrino masses, and a complex orthogonal matrix R. Thus, the effect of nonunitarity can easily be incorporated through the dependence of y_ν on $U_{\rm PMNS}$. The author of Ref. [35] has studied the effect of nonunitarity in leptogenesis following this approach in the context of a variant of a type-I seesaw. In that model, the sources of nonunitarity and active light neutrino mass generation were decoupled in the sense that the nonunitarity was due to the mixing of active neutrinos with neutral fermions that were different from the ones that were responsible for light neutrino mass generations. In this work, we study the effects of an eV scale sterile neutrino with large active-sterile mixing to explain the LSND-MiniBooNE anomaly on leptogenesis. In our analysis, we find that the contribution to the CP asymmetry from the nonunitary part is comparable to the one due to the unitary part, making the inclusion of nonunitary effects important. The parameter space that can give rise to successful leptogenesis gets constrained by the bounds on the active-sterile mixing as obtained from the global analysis and thereby manifesting the effect of the light-sterile neutrino.

The rest of this paper is organized as follows: In Sec. II, the MES model is briefly reviewed, and the CI parametrization for the neutrino Dirac Yukawa couplings is discussed in Sec. III. The basics of leptogenesis and the relevant working formulas are given in Sec. IV. The results of our analysis are discussed in Sec. V and we conclude in Sec. VI.

II. THE MINIMAL EXTENDED SEESAW

In the MES model [26], one adds three RHNs ν_R and one sterile neutrino ν_s to the SM particle content. The part of the Lagrangian relevant for neutrino mass generation is

$$-\mathcal{L}_Y = y_\nu \bar{l}_L \tilde{H} \nu_R + \bar{\nu}_R^c M_S \nu_s + \frac{1}{2}\bar{\nu}_R^c M_R \nu_R + \text{H.c.}, \tag{2.1}$$

where l_L is the lepton doublet and H is the SM Higgs doublet with $\tilde{H} = i\sigma_2 H^*$. Note that, in the above equation, the generation indices are suppressed and y_ν is the 3×3 neutrino Yukawa coupling matrix, and M_S and M_R are 3×1 and 3×3 matrices respectively. Without loss of generality, we work in a basis in which M_R is diagonal and real. We also take the charged lepton mass matrix to be diagonal. Once the electroweak symmetry is spontaneously broken, the Lagrangian in Eq. (2.1) becomes

$$\mathcal{L}_\nu = \bar{\nu}_L M_D \nu_R + \bar{\nu}_R^c M_S \nu_s + \frac{1}{2}\bar{\nu}_R^c M_R \nu_R + \text{H.c.}, \tag{2.2}$$

where $M_D = y_\nu v/\sqrt{2}$ and $v = 246$ GeV is the Higgs vacuum expectation value. The Lagrangian in Eq. (2.2) leads to the following 7×7 neutrino mass matrix in the $(\nu_L, \nu_s^c, \nu_R^c)$ basis:

$$M_\nu^{7\times 7} = \begin{pmatrix} 0 & 0 & M_D \\ 0 & 0 & M_S^T \\ M_D^T & M_S & M_R \end{pmatrix}. \tag{2.3}$$

Assuming the mass terms to have a hierarchy as $M_R \gg M_S > M_D$, the RHNs that are much heavier compared to v can be integrated out first. This results in the effective 4×4 light neutrino mass matrix in the (ν_L, ν_s^c) basis, which is given as

$$M_\nu^{4\times4} = -\begin{pmatrix} M_D M_R^{-1} M_D^T & M_D M_R^{-1} M_S^T \\ M_S (M_R^{-1})^T M_D^T & M_S M_R^{-1} M_S^T \end{pmatrix}. \quad (2.4)$$

This is a minimal extension of the type-I seesaw in the sense that only one extra sterile field is added to the standard type-I seesaw scenario and the mass of this additional sterile field is also suppressed by M_R along with that of the three active neutrinos. Since $M_\nu^{7\times7}$ has rank 6 and, subsequently, $M_\nu^{4\times4}$ has rank 3, the lightest neutrino state becomes massless. Now, since $M_S > M_D$, one may further integrate out the eV scale sterile state ν_s of mass

$$m_4 \simeq M_S M_R^{-1} M_S^T \quad (2.5)$$

from Eq. (2.4) to get the 3×3 active light neutrino mass matrix as

$$M_\nu^{3\times3} \simeq M_D M_R^{-1} M_S^T (M_S M_R^{-1} M_S^T)^{-1} M_S M_R^{-1} M_D^T - M_D M_R^{-1} M_D^T. \quad (2.6)$$

It is worth mentioning that the rhs of Eq. (2.6) remains nonvanishing since M_S is a row vector and not a square matrix. In the standard picture with three active light Majorana neutrino mixing, the relationship between the flavor and mass states is described by a 3×3 unitary matrix U_ν, which can be parametrized in terms of three mixing angles (θ_{12}, θ_{23}, and θ_{13}), one CP-violating phase (δ), and two Majorana phases (α, β). (In our case, the lightest active neutrino is massless and this implies that $\beta = -\alpha$.) Adding a sterile state expands the mixing matrix to 4×4, in which the added degrees of freedom can be parametrized by introducing three new rotation angles (θ_{14}, θ_{24}, and θ_{34}) and two new oscillation-accessible CP-violating phases, δ_{14} and δ_{24}. In fact, in the above step of integrating out the eV scale sterile neutrino, the mass matrix in Eq. (2.4) can be diagonalized by the 4×4 unitary matrix that is given as (since we are neglecting the nonunitarity due to ν_R, which goes as $M_D^2/M_R^2 \sim 10^{-20}$ taking $M_D \sim 100$ and $M_R \sim 10^{12}$ GeV)

$$U \simeq \begin{pmatrix} (1 - \frac{1}{2} V V^\dagger) U_\nu & V \\ -V^\dagger U_\nu & 1 - \frac{1}{2} V^\dagger V \end{pmatrix}. \quad (2.7)$$

In this equation, the three-component column vector V is given by

$$V = M_D M_R^{-1} M_S^T (M_S M_R^{-1} M_S^T)^{-1} \equiv (U_{e4}, U_{\mu4}, U_{\tau4})^T, \quad (2.8)$$

and it corresponds to the active-sterile mixing, which is responsible for the nonunitarity of the PMNS matrix,

$$U_{\rm PMNS} = \left(1 - \frac{1}{2} V V^\dagger\right) U_\nu. \quad (2.9)$$

Here, U_ν is the 3×3 unitary PMNS matrix. Note that V is suppressed by $\mathcal{O}(M_D/M_S)$ and hence the deviation of $U_{\rm PMNS}$ from unitarity, i.e., $-\frac{1}{2} U_L V V^\dagger U_\nu$, is $\sim\mathcal{O}(M_D^2/M_S^2)$.

III. CASAS-IBARRA PARAMETRIZATION FOR THE YUKAWA COUPLINGS

Using the CI parametrization [34], one can express the Dirac mass matrix in terms of the $U_{\rm PMNS}$ matrix, the light and heavy neutrino masses, and a complex orthogonal matrix R. In this section, we derive the CI parametrization for the Dirac mass matrix M_D in the MES model. To do this, note that the light neutrino mass matrix in Eq. (2.6) can be written as

$$M_\nu^{3\times3} \simeq M_D (M_R^{-1} M_S^T (M_S M_R^{-1} M_S^T)^{-1} M_S M_R^{-1} - M_R^{-1}) M_D^T = M_D A M_D^T, \quad (3.1)$$

where we have denoted

$$A = M_R^{-1} M_S^T (M_S M_R^{-1} M_S^T)^{-1} M_S M_R^{-1} - M_R^{-1}, \quad (3.2)$$

which is a 3×3 symmetric matrix. Now, $M_\nu^{3\times3}$ can be diagonalized as

$$U_{\rm PMNS}^T (M_\nu^{3\times3}) U_{\rm PMNS} \equiv U_{\rm PMNS}^T (M_D A M_D^T) U_{\rm PMNS} = D_m, \quad (3.3)$$

where

$$D_m = {\rm diag}(m_1, m_2, m_3), \quad (3.4)$$

and $m_{1,2,3}$ are the light neutrino masses. Writing Eq. (3.3) as

$$D_m = U_{\rm PMNS}^T M_D \sqrt{A} \sqrt{A} M_D^T U_{\rm PMNS}, \quad (3.5)$$

and multiplying the left and right of this equation by $\sqrt{D_m^{-1}}$, we get

$$I = \sqrt{D_m^{-1}} U_{\rm PMNS}^T M_D \sqrt{A} \sqrt{A} M_D^T U_{\rm PMNS} \sqrt{D_m^{-1}} = \left(\sqrt{A} M_D^T U_{\rm PMNS} \sqrt{D_m^{-1}}\right)^T \left(\sqrt{A} M_D^T U_{\rm PMNS} \sqrt{D_m^{-1}}\right). \quad (3.6)$$

Thus,

$$R = \sqrt{A} M_D^T U_{\rm PMNS} \sqrt{D_m^{-1}} \quad (3.7)$$

is a 3×3 orthogonal matrix. The above equation can be inverted to write M_D as

$$M_D^T = (\sqrt{A})^{-1} R \sqrt{D_m} U_{\rm PMNS}^{-1}, \quad \text{or}$$
$$M_D = U_{\rm PMNS}^{*} \sqrt{D_m} R^T (\sqrt{A})^{-1}. \tag{3.8}$$

This is the CI parametrization for M_D in the MES model. Note that, in the above equation, A is given by Eq. (3.2) and R is a general 3×3 complex orthogonal matrix. It is evident from the above expression that the scale of M_D is guided by the scales of M_S and M_R. Also, taking $U_{\rm PMNS} = (1 - \frac{1}{2} VV^\dagger) U_\nu$ in Eq. (3.8) will amount to incorporating the nonunitary effects (and hence both the dimension-five and dimension-six contributions to leptogenesis), whereas taking $U_{\rm PMNS} = U_\nu$ (an artificial case, where only the dimension-five contribution is taken by putting $V = 0$ by hand) will switch off the nonunitary effects.

IV. BARYOGENESIS THROUGH LEPTOGENESIS

It is well known that an out-of-equilibrium CP-violating decay of the RHNs in the early Universe can produce a lepton asymmetry, which, in turn, can be converted into the baryon asymmetry dynamically (for details, see [36–39]). In this paper, we focus on the vanilla leptogenesis in the context of the MES model. Leptogenesis in the MES scheme has been discussed in [40,41] with keV scale sterile neutrinos. As we will see in the next section, incorporating the bounds from oscillation experiments including the ones on active-sterile mixing would imply that $M_1 \gtrsim 10^{11}$ GeV with most of the points lying above 10^{12} GeV, which is the unflavored regime of leptogenesis. Thus, the expression for the CP asymmetry guided by the decay of the lightest RHN in this model can be written as [39]

$$\epsilon_1 = \frac{1}{8\pi v^2} \frac{1}{(M_D M_D^\dagger)_{11}} \sum_{j=2,3} \mathrm{Im}\{(M_D M_D^\dagger)_{1j}^2\} f(x), \tag{4.1}$$

where the loop function can be expressed as $f(x) = \sqrt{x}(1 - (1+x)\ln(\frac{1+x}{x}) - \frac{1}{1-x})$ with $x = \frac{M_j^2}{M_1^2}$. For $x \gg 1$, i.e., when a large hierarchy exists among the RHN mass states, one can simply write $f(x) \approx -\frac{3}{2\sqrt{x}}$. After determining the lepton asymmetry ϵ_1 using the above expression, the corresponding baryon asymmetry can be obtained through the electroweak sphaleron processes as [42,43]

$$Y_B = 1.27 \times 10^{-3} \epsilon_1 \eta(\tilde{m}_1). \tag{4.2}$$

Here, the factor

$$\tilde{m}_1 = (M_D M_D^\dagger)_{11} / M_1 \tag{4.3}$$

is a measure of the effective neutrino mass that contains the information on solar and atmospheric mass splittings. The nature of the washout regime is also decided by the efficiency factor η, which is as [39,44]

$$\eta(\tilde{m}_1) \approx 1/((8.25 \times 10^{-3}\ \text{eV})/\tilde{m}_1 + (\tilde{m}_1/(2 \times 10^{-4}\ \text{eV})^{1.16}). \tag{4.4}$$

Departure from thermal equilibrium[2] can be estimated by comparing the interaction rate with the expansion rate of the Universe. At very high temperatures $T \geq 10^{12}$ GeV, all charged lepton flavors are out of equilibrium, and hence all of them behave indistinguishably, resulting in the vanilla leptogenesis scenario. The decay parameter that governs the competition between the decay rate and expansion rate of the Universe can be written as

$$K = \frac{\Gamma_1}{H(T = M_1)} = \frac{(M_D M_D^\dagger)_{11} M_1}{8\pi v^2} \frac{M_{\rm pl}}{1.66\sqrt{g_*} M_1^2}, \tag{4.5}$$

where Γ_1 is the decay rate of the lightest RHN ν_{R1}, and $H(T = M_1)$ is the Hubble expansion rate at temperature $T = M_1$. The effective number of relativistic degrees of freedom is measured by the quantity g_*, which is 106.75 [46]. Depending on K, one can have an idea whether it is in agreement with Sakharov's third condition or not.

It is also instructive to examine the washout regime in the scenario of thermal leptogenesis, which relies on the parameter η as evident in Eq. (4.4). The efficiency factor is directly connected to K through the parameter $\tilde{m}$, which again depends on the order of neutrino mass-squared differences. In our analysis, the efficiency factor is obtained to be of the order of 10^{-4}–10^{-3}, which gives an insight into the amount of washout produced. This order of the washout strictly falls within the strong regime, which is also favored by the observed neutrino mass-squared differences [36].

V. NUMERICAL ANALYSIS AND RESULTS

In this section, we discuss the numerical analysis performed and the results obtained in detail. We investigate the parameter space that allows successful thermal leptogenesis, at the same time satisfying the bounds from the $3+1$ mixing data. An adequate amount of lepton asymmetry is essentially sourced by the complex Yukawa coupling (y_ν), which governs the RHN decay to the SM lepton and the Higgs doublet. As discussed above, the presence of additional sterile states in the seesaw mechanism induces deviation of the neutrino mixing matrix from being unitary. Note that the canonical type-I seesaw also admits nonunitarity and is determined by the factor M_D^2/M_R^2, which is very small [$\sim\mathcal{O}(10^{-20})$]. However, for the extended seesaw mechanism that has an additional eV sterile neutrino, the nonunitarity is determined by the ratio M_D^2/M_S^2, which can be $\sim\mathcal{O}(0.1)$. Assuming that such a sterile neutrino is responsible for the LSND-MiniBooNE anomalies, the results of the fit of short-baseline neutrino

[2]Which is Sakharov's third condition [45] to be satisfied to have a baryon asymmetry.

TABLE I. The 3σ ranges for the $3+1$ neutrino oscillation parameters [13,31,47,48] that are used in our analysis.

	3σ range
$\sin^2\theta_{12}$	$0.24 \to 0.377$
$\sin^2\theta_{13}$	$0.02044 \to 0.02437$
$\sin^2\theta_{23}$	$0.48 \to 0.599$
$\Delta m^2_{21}/\mathrm{eV}^2$	$6.79\times10^{-5} \to 8.01\times10^{-5}$
$\Delta m^2_{31}/\mathrm{eV}^2$	$2.431\times10^{-3} \to 2.622\times10^{-3}$
$\Delta m^2_{41}/\mathrm{eV}^2$	$0.87 \to 2.04$
$\lvert V_{e4}\rvert^2$	$0.012 \to 0.047$
$\lvert V_{\mu4}\rvert^2$	$0.005 \to 0.03$
$\lvert V_{\tau4}\rvert^2$	<0.16

oscillation data for the $3+1$ active-sterile neutrino mixing are given in Table I [13,31,47,48].

To find out the parameter space that gives the correct baryon asymmetry, we first determined the values of the Dirac mass matrices M_D (which is just $y_\nu v/\sqrt{2}$) that satisfies all the low energy data with the help of the CI parametrization discussed in Sec. III. For this, we did a random scanning over all the neutrino oscillation parameters in their 3σ ranges, which are given in Table I. Care has been taken to abide by the hierarchy of the mass scales as $M_D < M_S \ll M_R$, as is required for the MES model, thereby ensuring the validity of the seesaw approximations. This particular hierarchy among the mass scales not only ensures the light-sterile neutrino to have a mass in the eV regime, but also facilitates in maintaining the active-sterile mixing strength that is complied by the experimental data. We have taken only those points for which $\mathcal{O}(M_D) \le 0.1\mathcal{O}(M_S)$. We have neglected the next-to-leading-order corrections to the active neutrino mass matrix, which is of the order of $\frac{M_D^4}{M_S^2 M_R}$ [49], as it is always $\le 5\times10^{-5}$ in the parameter space that we have considered. In our scanning, we have chosen the following ranges for the entries of the corresponding mass matrices:

$$200 \le |M_S^{i1}| \le 3000\ \mathrm{GeV},$$
$$10^8 \le M_R^{ii} \le 10^{16}\ \mathrm{GeV} \qquad (i=1,2,3). \qquad (5.1)$$

We have chosen M_R to be diagonal and real, whereas for the 3×1 matrix M_S, phases of the entries are varied in the range $0-2\pi$. The Dirac and Majorana phases that enter U_ν are also varied in the ranges $0-2\pi$ and 0–π, respectively. These five phases act as the sources of CP violation (we have kept the orthogonal matrix R to be real for simplicity, with the angles varying in the range $0-2\pi$). Using these ranges and the 3σ oscillation parameters, we performed a random scanning over 3×10^8 data points to find out M_D (or y_ν) and then we calculated the baryon asymmetry Y_B using the expressions given in Sec. IV. To show the impact of the inclusion of the nonunitary corrections due to active-sterile mixing on the baryon asymmetry, we have given a few benchmark points in Table II. Four different points are given corresponding to different masses of the lightest heavy RHN, M_1. The third and the fifth columns show the values of Y_B calculated just from the unitary part and from the inclusion of nonunitary parts, respectively. The former is only an artificial case where we put the $V^\dagger V$ term as zero by hand, and hence it takes into account only the dimension-five contribution to Y_B. It can be seen that the inclusion of the $V^\dagger V$ term (which is the dimension-six contribution) has a considerable impact on Y_B and thereby indicates the dependence of Y_B on active-sterile mixing.

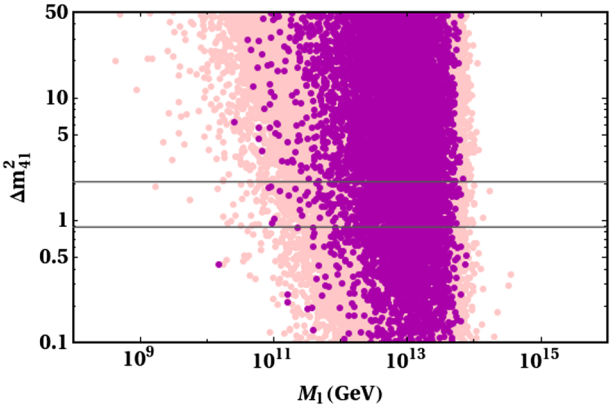

FIG. 1. Variation of Δm^2_{41} with respect to the mass of lightest RHN. The region within the gray lines corresponds to the range of Δm^2_{41} allowed by the experiments. The pink points do not satisfy the bounds on active-sterile mixing, but they satisfy the constraints from three neutrino masses and mixing. The magenta points satisfy the bounds on active-sterile mixing that are shown in Table I.

In Fig. 1, we have shown the variation of Δm^2_{41} with respect to the mass of the lightest RHN. Here, the region

TABLE II. Baryon (Y_B) and CP (ϵ_1) asymmetries with and without including the nonunitary corrections for different benchmark points.

M_1 (GeV)	m_{sterile} (eV)	Y_B (from unitary part)	ϵ_1 (from unitary part)	Y_B (total)	ϵ_1 (total)
4.2624×10^9	1.58356	2.07665×10^{-16}	1.38397×10^{-9}	7.91104×10^{-16}	4.1033×10^{-10}
4.32082×10^{10}	1.98397	6.23251×10^{-16}	3.6963×10^{-8}	2.45091×10^{-13}	3.80607×10^{-7}
1.01752×10^{12}	0.938872	2.93063×10^{-14}	9.77027×10^{-8}	9.32359×10^{-13}	1.22387×10^{-6}
1.00007×10^{13}	1.16399	3.29334×10^{-11}	0.000107207	1.29023×10^{-11}	3.43336×10^{-6}

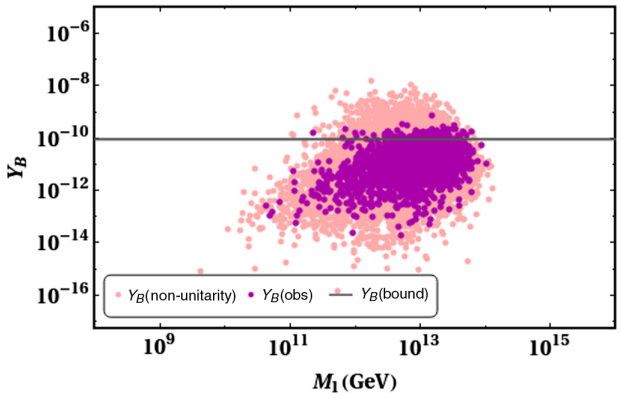

FIG. 2. Variation of Y_B with respect to the mass of lightest RHN. No constraints are put on the active-sterile mixing for the pink points, but these points satisfy the constraints on three neutrino mixing and have an eV scale sterile neutrino with Δm^2_{41} in the range 0.87–2.04 eV^2. The magenta points correspond to the parameter space where the active-sterile mixing complies with the experimental data. The gray thick line corresponds to the observed baryon asymmetry of the Universe.

within the gray lines corresponds to the range of Δm^2_{41} allowed by experiments (0.87–2.04 eV^2). The use of CI parametrization implies that the bounds from the three neutrinos mixing are satisfied. The pink points do not satisfy the bounds on active-sterile mixing, whereas the magenta points satisfy these bounds that are shown in Table I. Thus, one can note from this figure that the requirement of having an eV scale sterile neutrino itself imposes a lower bound on the value of M_1 as $\sim 10^{10}$ GeV, as can be seen from the region within the gray band. Once the bounds on active-sterile mixing are incorporated, this lower bound on M_1 increases further to $\sim 10^{11}$ GeV.

Figure 2 shows the variation of the baryon asymmetry yield with respect to the mass of the lightest RHN. In this figure, no constraints are put on the active-sterile mixing for the pink points, but they satisfy the constraints on three neutrino mixing and have an eV scale sterile neutrino with Δm^2_{41} in the range 0.87–2.04 eV^2. The magenta points correspond to the parameter space where the active-sterile mixing satisfies the bounds from the experimental data, as given in Table I. The gray thick line corresponds to the observed baryon asymmetry of the Universe,

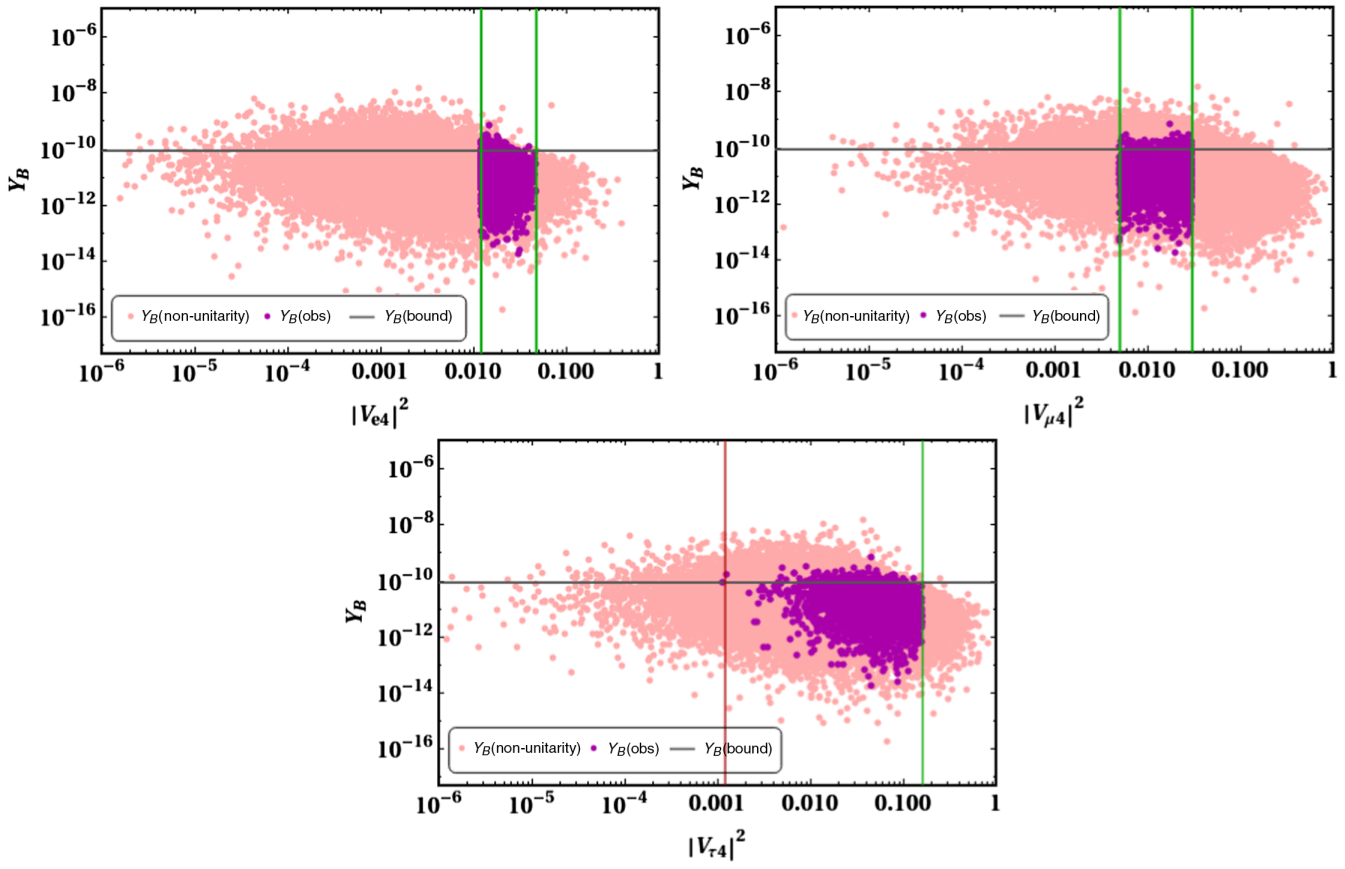

FIG. 3. Variation of Y_B with respect to the active-sterile mixing: $|V_{e4}|^2$, $|V_{\mu 4}|^2$, and $|V_{\tau 4}|^2$. The color codes are the same as in Fig. 2. The green lines are used to indicate the upper and/or lower bound of the matrix elements $|V_{\alpha 4}|^2$ provided by the relevant experiments. The red line shows the lower bound on $|V_{\tau 4}|^2$, which we have obtained from our analysis.

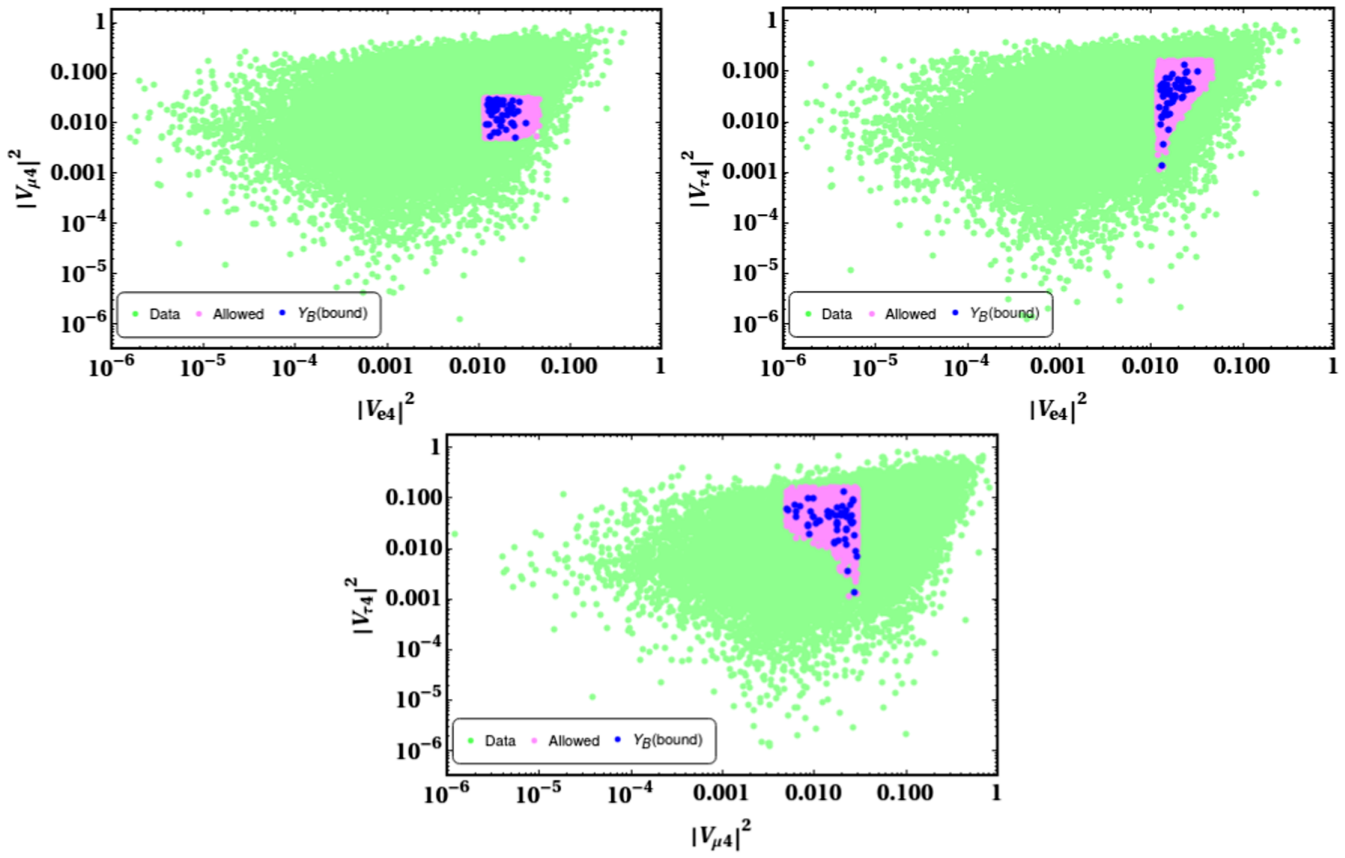

FIG. 4. Correlations among the active-sterile mixing elements by taking various constraints into account. The green region corresponds to the parameter space that satisfies the bounds from three neutrino mixing and there exists a light-sterile neutrino of mass in the range (0.87–2.04) eV^2. The pink points correspond to the parameter space that satisfies the bounds on the active-sterile mixing as shown in Table I. The blue points indicate the regions that give the correct values for the observed baryon asymmetry of the Universe, that is, in the range $Y_B = (8.52\text{–}8.93) \times 10^{-11}$.

$Y_B = (8.52\text{–}8.93) \times 10^{-11}$. We have seen from Fig. 1 that the model itself imposes a constraint on the mass of the lightest heavy RHN to be $M_1 \gtrsim 10^{11}$ GeV, once the bounds on the mass-squared difference and active-sterile mixing are incorporated. It can be seen from Fig. 2 that, for this model to account for the entire observed baryon asymmetry, M_1 has to be greater than 10^{11} GeV (the region where the thick gray line overlaps with the pink points). The value of M_1 is restricted further once the bounds on active-sterile mixing are included, as is shown by the magenta points (the region where the gray thick line overlaps with the magenta points). In fact, M_1 prefers to take values $\gtrsim 10^{12}$ GeV to give the correct baryon asymmetry. As mentioned earlier, this is the unflavored regime of leptogenesis where the flavors are indistinguishable. Note that this value of M_1 is higher than the Davidson-Ibarra bound of 10^8–10^9 GeV for the canonical type-I seesaw model [50].

In Fig. 3 , we show the variation of Y_B with respect to the three active-sterile mixing: $|V_{e4}|^2$ (upper left panel), $|V_{\mu 4}|^2$ (upper right panel), and $|V_{\tau 4}|^2$ (lower panel). The color codes are the same as in Fig. 2. The green lines are used to indicate the upper and/or lower bound of the mixing parameters from global analysis given in Table I . In our scanning, these parameters take values from 10^{-6} to 1 and the figures show that, even for very small values of these mixing parameters, successful baryogenesis can be obtained. The magenta points in the upper panels show that the constraint on Y_B is satisfied in the current allowed ranges of $|V_{e4}^2|$ and $|V_{\mu 4}^2|$. In the case of $|V_{\tau 4}|^2$, there exists no lower bound from the current experimental data and there is only an upper bound of 0.16. However, the model gives a lower bound on $|V_{\tau 4}|^2$ as $\sim$0.001. This lower bound is coming due to the large values of $|V_{e4}^2|$ and $|V_{\mu 4}^2|$ in the region allowed by the experiments. We can see from the figures that this lower bound on $|V_{\tau 4}|^2$ is not there once we let go of the bounds on the other two mixing elements, as is shown by the pink points.

In Fig. 4 , we present the correlations among the active-sterile mixing elements obtained from the imposition of the various constraints on the total parameter space. As seen earlier, there can be a large region of parameter space that obeys all the three-neutrino oscillation data as depicted by the green region in this figure. However, it is to be noted here that this is not the final parameter space we are looking

for. The pink points in this figure correspond to the parameter space that satisfies the bounds on the active-sterile mixing as shown in Table I and the blue points indicate the regions that give the correct values for the observed baryon asymmetry, that is, in the range $Y_B = (8.52\text{–}8.93) \times 10^{-11}$. We can clearly see the existence of a lower bound on $|V_{\tau 4}|^2$ as $\sim$0.001 in this model, once the bounds on $|V_{e4}|^2$ and $|V_{\mu 4}|^2$ are incorporated, as was seen in Fig. 3. In addition, there is no real correlation between $|V_{e4}|^2$ and $|V_{\mu 4}|^2$ in the parameter space allowed by the experiments (pink region of the upper left panel in Fig. 4). On the other hand, relatively higher values of $|V_{\tau 4}|^2$ are preferred for higher values of $|V_{e4}|^2$ (pink region of the upper right panel in Fig. 4) and lower values of $|V_{\mu 4}|^2$ (pink region of the lower panel in Fig. 4). Values of $|V_{\tau 4}|^2$ in the range $\sim$0.001–0.16 are allowed corresponding to the lower limit on $|V_{e4}|^2$ and upper limit on $|V_{\mu 4}|^2$, respectively. As can be seen from the blue points, successful baryogenesis is possible in most of the regions allowed by the experiments for the eV scale sterile neutrino.

VI. CONCLUSIONS

In this work, we have studied the effects of an eV scale sterile neutrino on leptogenesis in the context of the minimal extended seesaw model. This model contains a light-sterile neutrino, in addition to the three heavy Majorana right-handed neutrinos. Here, the active-light sterile mixing acts as nonunitary parameters, introducing considerable deviation of the PMNS matrix from being unitary. We noted that the constraints on the active-sterile mixing coming from global analysis of the data from various short-baseline experiments impose an upper bound on the lightest heavy neutrino mass scale (M_1) as $\gtrsim 10^{11}$ GeV in this model. This is an artifact of the modified expression for M_D, as well as the requirement of having an eV scale sterile neutrino. In addition, we also found that there exists a lower bound of $\sim$0.001 on the active-sterile mixing element $|V_{\tau 4}|^2$ once the bounds on $|V_{e4}|^2$ and $|V_{\mu 4}|^2$ are incorporated. This is an important prediction from the model since the analysis of current data only gives an upper bound of 0.16 on $|V_{\tau 4}|^2$.

Coming to the implications for leptogenesis, we studied the standard vanilla leptogenesis where the out-of-equilibrium decay of the heavy right-handed Majorana neutrinos in the early Universe can generate a lepton asymmetry, which, in turn, can be converted into a baryon asymmetry by the nonperturbative sphaleron processes. We used the Casas-Ibarra parametrization of the Dirac mass term for active neutrinos to facilitate our numerical analysis. We found that the incorporation of the bounds on active-sterile mixing raises the lower bound on M_1 to be $\gtrsim 10^{12}$ GeV and thereby makes the flavor effects on leptogenesis insignificant in this parameter space. Thus, we noted that, even though it might look as if the light-sterile neutrino plays no role in leptogenesis, the bounds on active-sterile mixing actually shrinks the parameter space where successful explanation of the observed baryon asymmetry of the Universe is possible. We have also studied the correlations of Y_B to the active-sterile mixing parameters and noted that successful baryogenesis is possible in most of the regions allowed by the experiments. In summary, the nonunitary effects in the MES model can give rise to interesting consequences for leptogenesis.

ACKNOWLEDGMENTS

S. G. acknowledges the J.C Bose Fellowship (JCB/2020/000011) of Science and Engineering Research Board of Department of Science and Technology, Government of India. A. M. would like to acknowledge the financial support provided by SERB-DST, Government of India through the Project No. EMR/2017/001434. A. M. also acknowledges the post doctoral fellowship offered by the Saha Institute of Nuclear Physics.

[1] A. Aguilar-Arevalo *et al.* (LSND Collaboration), Evidence for neutrino oscillations from the observation of anti-neutrino(electron) appearance in a anti-neutrino(muon) beam, Phys. Rev. D **64**, 112007 (2001).

[2] A. Aguilar-Arevalo *et al.* (MiniBooNE Collaboration), Significant Excess of Electronlike Events in the MiniBooNE Short-Baseline Neutrino Experiment, Phys. Rev. Lett. **121**, 221801 (2018).

[3] Y. Declais *et al.*, Search for neutrino oscillations at 15-meters, 40-meters, and 95-meters from a nuclear power reactor at Bugey, Nucl. Phys. **B434**, 503 (1995).

[4] G. Mention, M. Fechner, T. Lasserre, T. Mueller, D. Lhuillier, M. Cribier, and A. Letourneau, The reactor antineutrino anomaly, Phys. Rev. D **83**, 073006 (2011).

[5] P. Anselmann *et al.* (GALLEX Collaboration), First results from the Cr-51 neutrino source experiment with the GALLEX detector, Phys. Lett. B **342**, 440 (1995).

[6] W. Hampel *et al.* (GALLEX Collaboration), Final results of the Cr-51 neutrino source experiments in GALLEX, Phys. Lett. B **420**, 114 (1998).

[7] C. Giunti and M. Laveder, Statistical significance of the gallium anomaly, Phys. Rev. C **83**, 065504 (2011).

[8] D. Abdurashitov *et al.*, The Russian-American Gallium Experiment (SAGE) Cr Neutrino Source Measurement, Phys. Rev. Lett. **77**, 4708 (1996).
[9] J. M. Berryman, P. Coloma, P. Huber, T. Schwetz, and A. Zhou, Statistical significance of the sterile-neutrino hypothesis in the context of reactor and gallium data, J. High Energy Phys. 02 (**2022**) 055.
[10] S. Goswami, Accelerator, reactor, solar and atmospheric neutrino oscillation: Beyond three generations, Phys. Rev. D **55**, 2931 (1997).
[11] C. Giunti and T. Lasserre, eV-scale sterile neutrinos, Annu. Rev. Nucl. Part. Sci. **69**, 163 (2019).
[12] S. Gariazzo, C. Giunti, M. Laveder, and Y. F. Li, Updated global $3+1$ analysis of short-baseline neutrino oscillations, J. High Energy Phys. 06 (2017) 135.
[13] M. Dentler, A. Hernández-Cabezudo, J. Kopp, P. A. Machado, M. Maltoni, I. Martinez-Soler, and T. Schwetz, Updated global analysis of neutrino oscillations in the presence of eV-scale sterile neutrinos, J. High Energy Phys. 08 (2018) 010.
[14] B. Dasgupta and J. Kopp, Sterile neutrinos, Phys. Rep. **928**, 63 (2021).
[15] B. Dasgupta and J. Kopp, Cosmologically Safe eV-Scale Sterile Neutrinos and Improved Dark Matter Structure, Phys. Rev. Lett. **112**, 031803 (2014).
[16] F. Forastieri, M. Lattanzi, G. Mangano, A. Mirizzi, P. Natoli, and N. Saviano, Cosmic microwave background constraints on secret interactions among sterile neutrinos, J. Cosmol. Astropart. Phys. 07 (2017) 038.
[17] N. Song, M. C. Gonzalez-Garcia, and J. Salvado, Cosmological constraints with self-interacting sterile neutrinos, J. Cosmol. Astropart. Phys. 10 (**2018**) 055.
[18] X. Chu, B. Dasgupta, M. Dentler, J. Kopp, and N. Saviano, Sterile neutrinos with secret interactions-cosmological discord?, J. Cosmol. Astropart. Phys. 11 (2018) 049.
[19] M. Archidiacono, S. Gariazzo, C. Giunti, S. Hannestad, and T. Tram, Sterile neutrino self-interactions: H_0 tension and short-baseline anomalies, J. Cosmol. Astropart. Phys. 12 (2020) 029.
[20] C. A. Argüelles, I. Esteban, M. Hostert, K. J. Kelly, J. Kopp, P. A. N. Machado, I. Martinez-Soler, and Y. F. Perez-Gonzalez, MicroBooNE and the ν_e interpretation of the MiniBooNE low-energy excess, arXiv:2111.10359.
[21] P. B. Denton, Sterile neutrino searches with MicroBooNE: Electron neutrino disappearance, arXiv:2111.05793.
[22] E. J. Chun, A. S. Joshipura, and A. Y. Smirnov, Models of light singlet fermion and neutrino phenomenology, Phys. Lett. B **357**, 608 (1995).
[23] E. J. Chun, A. S. Joshipura, and A. Y. Smirnov, Quasi-Goldstone fermion as a sterile neutrino, Phys. Rev. D **54**, 4654 (1996).
[24] V. Barger, D. Marfatia, and K. Whisnant, LSND anomaly from *CPT* violation in four neutrino models, Phys. Lett. B **576**, 303 (2003).
[25] R. N. Mohapatra, Connecting bimaximal neutrino mixing to a light sterile neutrino, Phys. Rev. D **64**, 091301 (2001).
[26] J. Barry, W. Rodejohann, and H. Zhang, Light sterile neutrinos: Models and phenomenology, J. High Energy Phys. 07 (2011) 091.
[27] H. Zhang, Light sterile neutrino in the minimal extended seesaw, Phys. Lett. B **714**, 262 (2012).
[28] P. Das, A. Mukherjee, and M. K. Das, Active and sterile neutrino phenomenology with A_4 based minimal extended seesaw, Nucl. Phys. **B941**, 755 (2019).
[29] R. Krishnan, A. Mukherjee, and S. Goswami, Realization of the minimal extended seesaw mechanism and the TM_2 type neutrino mixing, J. High Energy Phys. 09 (2020) 050.
[30] M. Fukugita and T. Yanagida, Baryogenesis without grand unification, Phys. Lett. B **174**, 45 (1986).
[31] N. Aghanim *et al.* (Planck Collaboration), Planck 2018 results. VI. Cosmological parameters, Astron. Astrophys. **641**, A6 (2020).
[32] V. Rubakov and M. Shaposhnikov, Electroweak baryon number nonconservation in the early Universe and in high-energy collisions, Usp. Fiz. Nauk **166**, 493 (1996).
[33] S. Antusch, S. Blanchet, M. Blennow, and E. Fernandez-Martinez, Non-unitary leptonic mixing and leptogenesis, J. High Energy Phys. 01 (**2010**) 017.
[34] J. A. Casas and A. Ibarra, Oscillating neutrinos and $\mu \to e, \gamma$, Nucl. Phys. **B618**, 171 (2001).
[35] W. Rodejohann, Non-unitary lepton mixing matrix, leptogenesis and low energy *CP* violation, Europhys. Lett. **88**, 51001 (2009).
[36] W. Buchmuller, P. Di Bari, and M. Plumacher, Leptogenesis for pedestrians, Ann. Phys. (Amsterdam) **315**, 305 (2005).
[37] W. Buchmuller, P. Di Bari, and M. Plumacher, Some aspects of thermal leptogenesis, New J. Phys. **6**, 105 (2004).
[38] G. Giudice, A. Notari, M. Raidal, A. Riotto, and A. Strumia, Towards a complete theory of thermal leptogenesis in the SM and MSSM, Nucl. Phys. **B685**, 89 (2004).
[39] S. Davidson, E. Nardi, and Y. Nir, Leptogenesis, Phys. Rep. **466**, 105 (2008).
[40] P. Das and M. K. Das, Phenomenology of keV sterile neutrino in minimal extended seesaw, Int. J. Mod. Phys. A **35**, 2050125 (2020).
[41] P. Das, M. K. Das, and N. Khan, Five-zero texture in neutrino-dark matter model within the framework of minimal extended seesaw, Nucl. Phys. **B980**, 115810 (2022).
[42] J. M. Cline, K. Kainulainen, and K. A. Olive, Protecting the primordial baryon asymmetry from erasure by sphalerons, Phys. Rev. D **49**, 6394 (1994).
[43] M. D'Onofrio, K. Rummukainen, and A. Tranberg, The sphaleron rate through the electroweak cross-over, J. High Energy Phys. 08 (2012) 123.
[44] W. Rodejohann, Non-unitary PMNS matrix, leptogenesis and low energy *CP* violation, AIP Conf. Proc. **1222**, 93 (2010).
[45] A. D. Sakharov, Violation of *CP* invariance, C asymmetry, and baryon asymmetry of the Universe, Pis'ma Zh. Eksp. Teor. Fiz. **5**, 32 (1967).
[46] M. Bauer and T. Plehn, *Yet Another Introduction to Dark Matter: The Particle Physics Approach*, Lecture Notes in Physics Vol. 959 (Springer, New York, 2019).

[47] M. Aker *et al.* (KATRIN Collaboration), First operation of the KATRIN experiment with tritium, Eur. Phys. J. C **80**, 264 (2020).

[48] S. Gariazzo, C. Giunti, M. Laveder, Y. F. Li, and E. M. Zavanin, Light sterile neutrinos, J. Phys. G **43**, 033001 (2016).

[49] N. Nath, M. Ghosh, S. Goswami, and S. Gupta, Phenomenological study of extended seesaw model for light sterile neutrino, J. High Energy Phys. 03 (2017) 075.

[50] S. Davidson and A. Ibarra, A Lower bound on the right-handed neutrino mass from leptogenesis, Phys. Lett. B **535**, 25 (2002).